International Journal of GEOMATE, Sep., 2025 Vol.29, Issue 133, pp.97-105
ISSN: 2186-2982 (P), 2186-2990 (O), Japan, DOI: https://doi.org/10.21660/2025.133.5031
Geotechnique, Construction Materials and Environment

SOIL-WATER CHARACTERISTIC AND UNSATURATED PERMEABILITY OF ENGINEERED SOIL WITH MULTI-MODAL POROSITY

*Nurly Gofar[1], Alfrendo Satyanaga[2], and Tri Harianto[3]

[1]Department of Civil Engineering, Graduate Program, Universitas Bina Darma, Indonesia
[2]Department of Civil and Environmental Engineering, Nazarbayev University, Kazakhstan
[3]Department of Civil Engineering, Faculty of Engineering, Universitas Hasanuddin, Indonesia

*Corresponding Author, Received: 27 April 2025, Revised: 02 July 2025, Accepted: 06 July 2025

ABSTRACT: Slopes formed by residual tropical soil are prone to slope instability triggered by rainfall. Rainwater seeps into the soil, increasing the water content and reducing soil suction. Changes in water content and soil suction of unsaturated soil are best understood through unsaturated soil parameters, such as the soil-water characteristic curve (SWCC) and unsaturated permeability curve. While a great deal of study has been dedicated to unimodal and bimodal soils, little has been done on multi- or tri-modal soils. Multi-modal porosity soil refers to soil that contains a range of pore sizes—such as several micro- and macropores—that influence its hydraulic behavior and water retention characteristics. This research is conducted to investigate the correlation between the soil's multi-modal porosity, derived from particle size distribution (PSD), and its soil water characteristic curve (SWCC). Compacted soil samples of sand-kaolin (SK), sand-kaolin-mica (SKM), and sand-kaolin-activated carbon (SKAC) were studied. It was found that the drying SWCC of SK and SKM can be categorized as bimodal, while the drying SWCC of SKAC is trimodal. On the other hand, the wetting SWCCs of all three soil samples are of the unimodal type. In addition, SKAC has the lowest permeability throughout the suction range as compared to SKM and SKAC due to a higher percentage of fine particles.

Keywords: Unsaturated soil, SWCC, Unsaturated permeability, Multi-modal porosity, Pore-size distribution

1. INTRODUCTION

Problems of rainfall-induced slope instability are more significant in tropical and highly populated urban areas in Indonesia, partly due to climate change. Soil profile extending from the ground surface to the groundwater table is in unsaturated condition, having voids which are not fully occupied with water [1]. The water content in this zone is low in comparison to the water content in the saturated zone below it. It is subject to change with rainfall infiltration and the effect of drought. Therefore, the wet and dry seasons highly influence the unsaturated zone.

Climate change is expected to increase the severity of storms in the wet season and droughts in the dry season [2]. The rainfall is occurring more frequently and lasting longer during the wet season. Long-duration rainfall could lead to the occurrence of rainfall-induced slope failures. On the other hand, prolonged drought results in an increase in suction and the development of cracks on the soil surface [3].

The negative effects of climate change on soil slope could be mitigated through a comprehensive knowledge of the unsaturated soil properties, i.e., soil-water characteristic curve (SWCC) and unsaturated coefficient of permeability [4]. These hydraulic properties facilitate the understanding of changes in soil suction and shear strength of unsaturated soil during rainfall or evaporation [5]. Two parameters are significant in the SWCC and permeability function, i.e. field capacity and coefficient of saturated permeability (k_s). Field capacity relates to the porosity (n) of the soil, which is defined as the ratio of the volume of voids to the total volume of soil. The field capacity of the soil is equal to the amount of water that can fill the voids of the soil mass.

Pore structure largely influences the engineering and hydraulic properties of a porous soil [6]. There are two types of pores: macro pores (large pores) are open pores, consisting of blind and through pores, while micro pores (small pores) are closed pores. Soils with one pore series result in a unimodal soil.

Particle size distributions (PSD) of soils do not always show a unimodal curve. For example, gap-graded soil forms two curves that are referred to as bimodal soils [7]. Some bimodal soils with dual porosity have two-pore series, and their behaviors are controlled by large pores (coarse grains) and small pores (fine grains). This occurs when finer grains do not fill the large voids between the coarse soil particles. Consequently, the gap-graded soils are bimodal and produce bimodal SWCC.

Bimodal SWCC has two sub-curves with two air-entry values (AEV)s. The first AEV represents air entering the open pores (macro pores) and water draining out from the open pores. The second AEV represents air entering closed pores (micro-pores), and water is drained out of the closed pores, which are surrounded by clay-sized particles [8].

SWCC is typically determined using laboratory testing methods, which include the pressure plate, Tempe cell, and centrifuge. However, these experimental data will only provide a few discrete data points along the drying and wetting SWCC curve. Therefore, Fredlund and Xing [9] best-fitting equation, which was developed using the least squares method, is required to produce a continuous SWCC for unimodal soils. The best fitting equation SWCC curve for soil with bimodal features was suggested by Satyanaga et al. [10, 11]. These equations are considered meaningful as the important parameters, such as the AEV of soils, have physical meanings. In these equations, the amount of water content in the soil reached zero when the suction of the soil reached 10^6 kPa.

The best fitting SWCC equation for bimodal soil proposed by Satyanaga et al. [10] is as follows:

$$\theta_w = (1 - \frac{ln(1+\frac{\psi}{\psi_r})}{ln(1+\frac{10^6}{\psi_r})})[\theta_r + (\theta_{s1} - \theta_{s2})(1 - erfc\frac{ln(\frac{\psi_{a1}-\psi}{\psi_{a1}-\psi_{m1}})}{s_1}) + (\theta_{s2} - \theta_r)(1 - erfc\frac{ln(\frac{\psi_{a2}-\psi}{\psi_{a2}-\psi_{m2}})}{s_2})] \quad (1)$$

where: θ_w = calculated volumetric water content, θ_s = saturated volumetric water content, ψ = matric suction, ψ_a = air-entry value of soil, ψ_m = matric suction at the inflection point of SWCC, θ_r = residual volumetric water content, ψ_r = matric suction corresponding to residual volumetric water content.

$$s_i = (\theta_{si})\, exp\sqrt{\frac{\sum_{i=1}^{n}(ln\frac{\psi_i}{\mu})}{n}} \quad (2)$$

where:

μ = geometric mean of matric suction.

$$\mu = \sqrt[n]{\psi_1\psi_2\psi_3...\psi_n} \quad (3)$$

Complementary error function =

$$erfc = \int_{-\infty}^{x} \frac{1}{\sqrt{2\pi}} \exp(-\frac{x^2}{2})dx \quad (4)$$

Multi-modal porosity soil refers to soil that contains a range of pore sizes—such as several micro- and macropores—that influence its hydraulic behavior and water retention characteristics. SWCCs with trimodal or multi-modal characteristics require two or more bimodal equations to best fit. Thus, an equation to best-fit a trimodal soil was proposed as an extension of Satyanaga et al.'s best-fit equation for bimodal SWCC is given in Eq. 5. In this equation, subscripts 1, 2, and 3 are associated with sub-curves 1, 2, and 3 in the SWCC with trimodal characteristics. The shape of trimodal SWCC and the parameters of the proposed SWCC equation are illustrated in Fig.1.

$$\theta_w = (1 - \frac{ln(1+\frac{\psi}{\psi_r})}{ln(1+\frac{10^6}{\psi_r})})[\theta_r + (\theta_{s1} - \theta_{s2})(1 - erfc\frac{ln(\frac{\psi_{a1}-\psi}{\psi_{a1}-\psi_{m1}})}{s_1}) + (\theta_{s2} - \theta_{s3})(1 - erfc\frac{ln(\frac{\psi_{a2}-\psi}{\psi_{a2}-\psi_{m2}})}{s_2}) + (\theta_{s3} - \theta_r)(1 - erfc\frac{ln(\frac{\psi_{a3}-\psi}{\psi_{a3}-\psi_{m3}})}{s_3})] \quad (5)$$

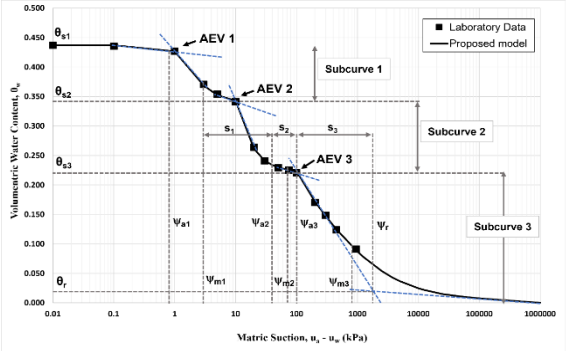

Fig. 1. SWCC with trimodal characteristics, with the definition of important parameters

The results of SWCC tests are presented in terms of gravimetric water content. A shrinkage curve is required to illustrate the relationship between gravimetric water content and void ratio as a soil specimen changes in volume with changes in the soil's moisture. It is used to convert the w-SWCC to the θ_w-SWCC and S_r-SWCC plots, incorporating the effect of volume change. Fredlund et al. [12] equation. Eq. 6 was adopted to represent the shrinkage curve in this study.

$$e(w) = a_{sh}\left[\frac{w^{c_{sh}}}{(b_{sh})^{c_{sh}}} + 1\right]^{\frac{1}{c_{sh}}} \quad (6)$$

where:

e(w)=the void ratio of the soil at a gravimetric water content, a_{sh} = minimum void ratio (e_{min}); b_{sh} = slope of the line of tangency, c_{sh} = curvature of shrinkage curve.

In general, the SWCC was obtained for dry conditions. However, to closely model the wetting process during the rainy season and drying process during the drought season, it is important to have SWCC curves for both conditions [13, 14].

Permeability is the measure of the ease of movement of water within soil. As water content is not constant for unsaturated soil, the unsaturated permeability establishes a relationship between soil's

permeability and soil suction. When soil suction is applied beyond the AEV, air displaces water from the pores and reduces the availability of water-filled pores. Given that water is only able to flow through water-filled pores, the permeability of the soil decreases. Thus, unsaturated permeability is also governed by soil suction [15].

It is postulated that compacted engineered soils with multi-modal porosity are less susceptible to changes in the external environment (prolonged drying and intense rainfall). If the postulation is correct, multi-modal soils would be beneficial for plant health because they can retain more water during prolonged drying and drain out water faster during intense rainfall [3].

This study uses compacted engineered soil samples created by mixing sand with kaolin, mica, and activated carbon to produce samples with gap-graded particle size distribution.

Sand was used as the coarse fraction for the mixture. Kaolin clay worked as the fine fraction to fill in the voids of the coarse sand [16]. The addition of kaolin can improve the workability of sand mixes by acting as a lubricant, making it easier to handle and shape.

Coarse muscovite (mica) has a two-dimensional sheet or layer structure, which is light colored. Naturally, mica can be found in residual soil from weathered granite [17]. A previous study involving mica was conducted by Priono et al. [18], which indicated that the addition of platy-shaped mica in sand-kaolin soil mixture altered the soil structure and the packing of soil particles. This resulted in a bimodal drying SWCC. Moreover, mica affects the hydraulic anisotropy of soil.

Powdered activated carbon is a porous carbon material that is widely used as an adsorbent to remove contaminants from both gases and liquids. The average particle diameter of the granular material is between 15 and 25 μm. The particles possess a large external surface-to-volume ratio and a high rate of adsorption. Adsorption is a surface phenomenon when a fluid is attracted to the surface of the adsorbent and forms an attachment by physical or chemical bonds [19]. Activated carbon has intrapores (structural pores), which are pores that are inside the activated carbon particle. The intra-pores could be further divided into three groups: intra-micropore, intra-mesopore, and intra-macropore. The adsorption of water by activated carbon is pressure dependent, as shown by the adsorption isotherms [20]. At low-to-moderate relative pressure, the adsorption of water by activated carbon is negligible; at high relative pressures, the adsorption of water begins to increase significantly due to micro-pore filling [21].

Recent studies have highlighted the significant influence of additive microstructure—particularly platy particles and intrapore materials—on the development of bimodal and trimodal soil-water characteristic curves (SWCCs). For instance, [22] and others have shown that biochar-amended soils exhibit heterogeneous and multimodal pore-size distributions, with intrapores contributing significantly to additional suction peaks and enhanced water retention. Complementary findings by [23] further confirmed that the inclusion of hydrochar, structurally analogous to activated carbon, leads to clearly delineated micro- and macropore regions in the SWCC, with altered hysteresis behavior. [24] further confirmed through greenhouse experiments and meta-analysis, respectively, that biochar or organic amendments enhance multimodal retention characteristics by modifying micro- and mesopore populations. Collectively, these studies support the hypothesis that materials such as mica and activated carbon can meaningfully modify the pore structure of soils, promoting bimodal or trimodal water retention behavior through their platy geometry and intrapore architecture.

2. RESEARCH SIGNIFICANCE

This research addresses a critical gap in unsaturated soil mechanics by exploring the hydraulic behavior of multi-modal porosity soils, a topic rarely investigated compared to unimodal or bimodal systems. The study's novelty lies in correlating particle size distribution with soil-water characteristic curves (SWCC) in engineered mixtures, revealing that SKAC exhibits a unique trimodal drying SWCC. Additionally, the contrast between drying (multi-modal) and wetting (unimodal) curves across all samples offers new insights into hysteresis behavior in compacted residual soils. These findings provide a more comprehensive understanding of hydraulic responses in tropical residual soils, advancing slope stability assessment under rainfall conditions.

3. MATERIALS AND METHODS

3.1 Materials

Three samples were used in this study, i.e., sand-kaolin (SK), sand-kaolin-mica (SKM), and sand-kaolin-activated carbon (SKAC). Previous research [20] indicated that the addition of coarse mica (muscovite) to the sand-kaolin increased the likelihood of obtaining a bimodal SWCC curve. Activated carbon could be derived from biochar, which has inter-pores (pore spaces between particles) and intra-pores (pores within the biochar) [22]. Thus, a small percentage of mica scraps and activated carbon were used to enhance the bimodality of the soil.

Fig. 2 visualizes the materials used in this study, while the compositions of the materials for specimens are given in Table 1.

Fig. 2 Materials used in this study

Table 1 Material composition

No	Soil Specimens' Composition (% by mass)	Specimen Designation
1	60% Ottawa Sand, 40% Kaolin	SK
2	54.5% Ottawa Sand, 36.4% Kaolin, 9.1% Coarse Mica	SKM
3	54.5% Ottawa Sand, 36.4% Kaolin, 9.1% Activated Carbon	SKAC

3.2 Methods

The index property tests and compaction tests of the samples were performed following ASTM standards. Static compaction was conducted to make identical specimens, 50 mm in diameter and 30 mm in height, with the same initial conditions to establish homogeneity across the different tests conducted. The soil mixture was split into three equal parts according to the mass of the targeted 95% maximum dry density at the dry of optimum. Subsequently, static compaction was carried out following ASTM D1883-21. The assigned amount of soil mixtures was compacted with a speed of 1.27 mm/min in three layers of 10 mm thick. The compacted soil samples were extruded, followed by the measurement of the diameter and height. The sample was weighted to obtain the mass. Moreover, the water content was measured on the soil mixture to establish the initial water content of the soil sample.

The Tempe cell and pressure plate are the most commonly used apparatus to determine SWCC using the axis-translation method [27]. Air pressure was applied within the Tempe cell and the pressure plate. The bottom of the high-air entry ceramic disk was attached to a water burette in atmospheric conditions. Given that the water pressure below the ceramic disk was atmospheric, the applied air pressure corresponds to the applied matric suction. The application of matric suction through the applied air pressure establishes the equilibrium water contents in the soil specimen, which follows criteria of mass change <0.1% over 24 hours [5]. For each applied pressure, the mass of soil specimens was weighed every day until the mass of water in the plotted graph had equalized. Subsequently, the matric suction was increased, and the procedure was repeated.

The shrinkage test was conducted by air-drying the specimens at room temperature (20–25°C) under controlled laboratory conditions. The dimensions of each specimen were 50 mm in diameter and 20 mm in height. The masses, heights, and diameters along four different axes were recorded daily using a precise weighing balance and a vernier caliper. Subsequently, the average volume and mass were plotted and best fitted using the equation presented in [12].

Mass and volume measurements were taken every 30 to 60 minutes during the early stages of drying and every 2 to 4 hours as the rate of moisture loss decreased, continuing until the weight stabilized over successive readings (usually 2–7 days). Once the decreases in volume and mass became negligible, the soil specimens were oven-dried at 105°C to obtain the mass of soil solids. The water content and void ratio for each reading were determined using the concept of mass and volume phase relationships.

4. RESULTS AND DISCUSSION

4.1. Properties of soil specimens

Table 2 summarizes the index properties of the soil specimen used in this study, while Fig. 3 shows the particle size distributions (PSD) of the three samples. The samples contain medium sands with about 40% of silt and clay particles. The curves in Fig. 3 represent gap-graded materials, which may result in bimodal or trimodal SWCC [6].

Table 2. Index properties of the soil specimen

Index Properties	SK	SKM	SKAC
USCS	SM	SM	SM
Bulk density, Mg/m^3	1.890	1.804	1.747
Specific Gravity, *Gs*	2.65	2.67	2.41
Liquid Limit, *LL*, %	53	50	56
Plastic Limit, *PL*, %	30	30	36
Plasticity Index PI, %	23	20	20
Coef. of sat. permeability, k_s, m/s	$6.65\ 10^{-6}$	$4.08\ 10^{-7}$	$1.47\ 10^{-7}$

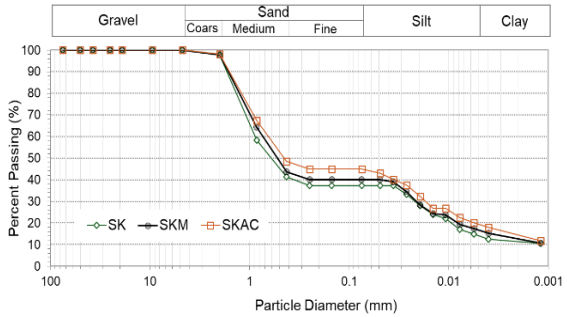

Fig.3 Particle size distribution of SK, SKM and SKAC

Fig. 4 shows the compaction curve of the soil specimens, SK, SKM, and SKAC. In addition, the maximum dry density, optimum water content, 95% of the maximum dry density at the dry of optimum, and the corresponding water content are listed in Table 3.

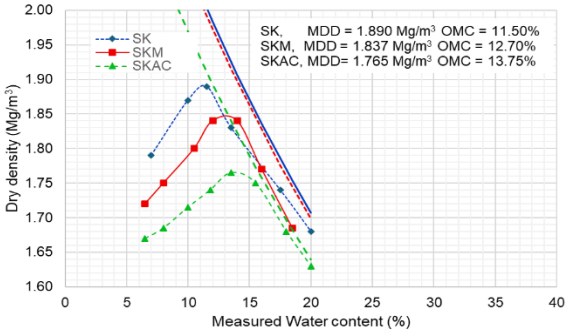

Fig. 4 Compaction curve of SK, SKM and SKAC

Table 3. Density and water content for specimen preparation

Sample	MDD g/m^3	OMC %	95% MDD Mg/m^3	Water content at 95% MDD %
SK	1.890	11.50	1.796	7.25
SKM	1.837	12.70	1.745	7.50
SKAC	1.765	13.75	1.677	7.30

4.2 Soil Water Characteristic Curves (SWCC)

Laboratory data for wetting and drying cycle SWCC of SK, SKM, and SKAC, obtained in terms of gravimetric water content (*w*), are presented in Figs. 5, 6, and 7. For the drying cycle, soil specimens SK and SKM exhibited bimodal SWCC, while SKAC exhibited trimodal SWCC. The best-fitting equations used were Satyanaga et al. [10] equation for bimodal SWCC and the extension of the equation presented in this paper for trimodal SWCC, respectively. For the wetting cycle, all three soil specimens, SK, SKM, and SKAC, exhibited unimodal SWCC and were best fitted using Fredlund and Xing's [9] equation.

SWCCs are normally presented in terms of volumetric water content. Therefore, the ordinate of Figs 5, 6, and 7 should be transformed to volumetric water content. In this case, a correction in volume should be made through a shrinkage curve, which represents the relationship between the void ratio (*e*) and gravimetric water content (*w*). The maximum volumetric water content is equal to the porosity of the soil ($n = e/(1+e)$). Figs. 8, 9, and 10 show the shrinkage curves for SK, SKM, and SKAC based on laboratory data and the curve fitting equation [12].

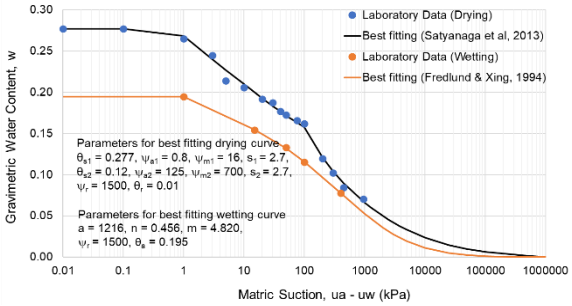

Fig. 5 SWCC for drying and wetting SK in terms of gravimetric water content

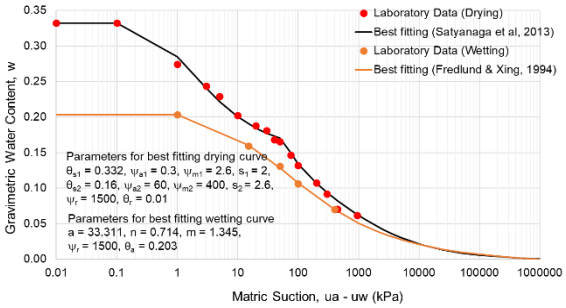

Fig. 6 SWCC for drying and wetting SKM in terms of gravimetric water content

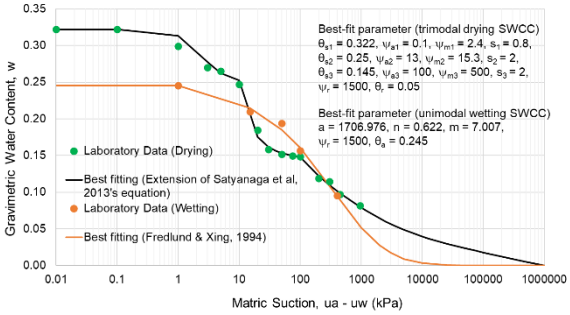

Fig. 7 SWCC for drying and wetting SKAC in terms of gravimetric water content

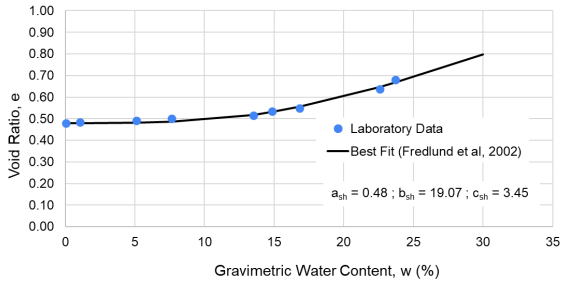

Fig. 8 Result of the shrinkage test for SK

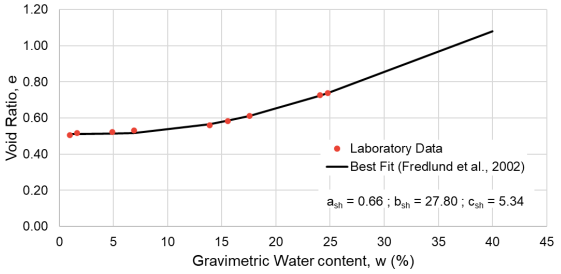

Fig. 9 Result of the shrinkage test for SKM

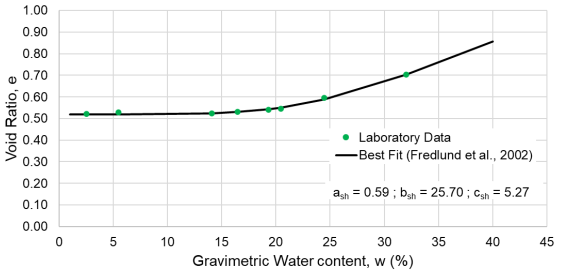

Fig. 10 Result of the shrinkage test for SKAC

Figs. 11, 12, and 13 show the SWCC of SK, SKM, and SKAC in terms of volumetric water content. Comparison of Figs 11, 12, and 13 with Figs. 5, 6, and 7 indicate that the consideration of shrinkage curves for SK, SKM, and SKAC only slightly changes the shape of the curves and fitting parameters because the samples used in this study are compacted engineered soils. The difference could be more significant for natural soil with large volume change, such as expansive soil.

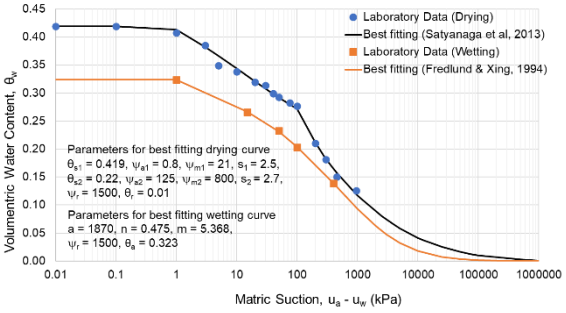

Fig. 11 SWCC for drying and wetting SK in terms of volumetric water content

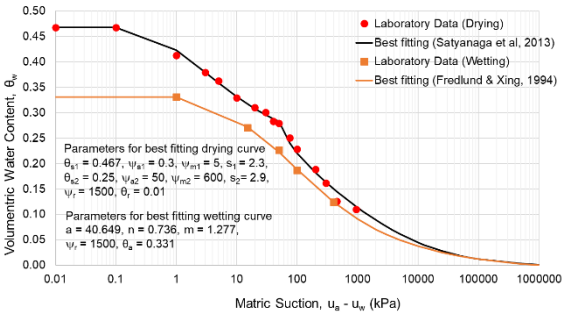

Fig. 12 SWCC for drying and wetting SKM in terms of volumetric water content

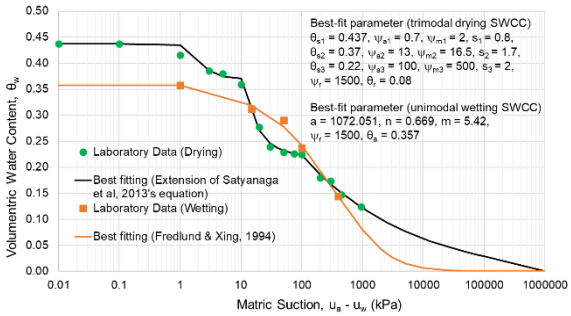

Fig. 13 SWCC for drying and wetting SKAC in terms of volumetric water content

Soil specimens SK and SKM exhibited bimodal SWCC for the drying cycle, which is caused by the bimodal pore-size distribution (PSD). The PSD shows two humps which concentrate around two pore sizes. At low matric suctions, water would be drained out from the large (macro) pores, and as matric suction increases, water would be drained out from the small (micro) pores. This is in agreement with previous studies [10]. SKAC exhibited trimodal drying SWCC. This may be attributed to the physical characteristics of activated carbon, which has intra-pores (pores inside the activated carbon particle), in addition to inter-pores between particles – macro pores and micro pores.

Based on Figures 5, 6, and 7, the first AEVs of the soil specimens (SK, SKM, and SKC) are between 0.3 kPa and 0.8 kPa, which are within the threshold of macropore (>50 μm). The peak of the curves corresponds to the dominant pore sizes at the corresponding AEV. For SK, the second peak pore radius of around 1.65 μm corresponds to the second AEV of 125 kPa, which is within the threshold of micropore (<5 μm). For SKM, the peak pore radii of around 143 μm (within the threshold of macropore, >50 μm) and 1.65 μm (within the threshold of micropore, <5 μm) correspond to the first and second AEV of 0.3 kPa and 50 kPa, respectively. For SKAC, the peak pore radii of around 143 μm, 3 μm, and 1.65 μm correspond to the first, second, and third AEV of 0.7 kPa, 13 kPa, and 100 kPa, respectively. The third AEV is possibly associated with the presence of the activated carbon's intra-micropores (<2 nm) attributed to its adsorption isotherms. Furthermore, SKM has the highest saturated volumetric water content θ_{s1} (0.467), followed by SKAC (0.437) and SK (0.419). SKM has the highest porosity (45.87%), followed by SKAC (43.44%) and SK (38.15%). As porosity is the ratio of volume of voids to total volume of the soil specimen, SKM has the highest volume of water filling the voids when saturated, resulting in the highest saturated volumetric water content compared to SK and SKAC.

While the drying SWCC exhibits bimodal and trimodal characteristics, the wetting SWCC for all three specimens exhibits unimodal characteristics. Furthermore, all the specimens are consistent in

showing that the saturated volumetric water content for the wetting curve is lower than that of the saturated volumetric water content for the drying curve, which is in agreement with the concept of hysteresis. This may be attributed to the reordering of soil solids and the presence of entrapped air in the pores of the soil specimen [5]. During the first desorption, air enters the soil pores, and the total soil specimen volume decreases (shrinkage). This may result in the reordering of the soil solids and the occlusion of soil pores, causing air to be entrapped in the pores of the soil specimens. The entrapped air within the soil solids reduces the total interconnected pore volumes. As the soil specimen is unable to absorb the same amount of water during the wetting cycle, a combination of these factors causes the wetting SWCC to be unimodal. Hysteresis is normally observed during desorption and adsorption cycles of SWCC, i.e., water content at the desorption curve is higher than that at the adsorption curve for the entire matric suction range [4]. However, for the SWCC of SKAC specimens, the adsorption cycle is higher than that of the desorption cycle (between matric suction 15 and 400 kPa).

The observed phenomenon wherein the wetting SWCC of SKAC exceeds the drying curve within the suction range of 15–400 kPa (Fig. 13) contradicts classical soil-water hysteresis behavior. This deviation suggests the presence of non-conventional mechanisms influencing water retention. One plausible explanation that warrants further investigation is the potential hydrophobic behavior of activated carbon under varying suction levels. Since the surface properties of activated carbon, including hydrophobicity or changes in surface energy, can significantly affect moisture adsorption and desorption characteristics, future studies can be carried out to explore the influence of such physico-chemical properties on SWCC hysteresis in SKAC. A deeper understanding in this regard could elucidate the anomalous trend and contribute to a more accurate modeling of water retention in activated carbon-amended soils.

4.3 Permeability Curves

The drying and wetting permeability functions of SK, SKM, and SKAC were developed using the statistical approach and are shown in Figs. 14, 15, and 16. As shown in Table 2, SKAC has the lowest saturated coefficient of permeability (1.47 10^{-7} m/s) compared to SK (6.65 10^{-6} m/s), and SKM (4.08 10^{-7} m/s). This could be explained by SKAC having the highest percentage of fines (42.68%) compared to SK (40.33%) and SKM (37.33%). The experimental results are in agreement in that a soil sample with higher fines content has lower permeability. It is expected that the permeability of SKM to be higher than SK due to the lower percentage of fines; however, it is observed that the permeability of SKM is lower than that of SK. This may be attributed to mica having a sheet or layer structure [17], which might alter the sand-kaolin-mica particle arrangement compared to the uniform sand-kaolin particle arrangement of SK. Consequently, the platy-shaped mica might disrupt the interconnectedness of the pore spaces for water to flow through, resulting in a lower permeability of SKM compared to SK. Furthermore, this could also be explained by the significant hydraulic anisotropy of SKM (10.47) [17]. The soil specimen SKM is comparable to that in the previous research [18], as both have a similar mica composition of 9%. As the saturated permeability is affected by the orientation and layering of soil specimens, the SKM would have exhibited a higher saturated permeability by approximately one order if the specimen were vertically layered rather than horizontally layered.

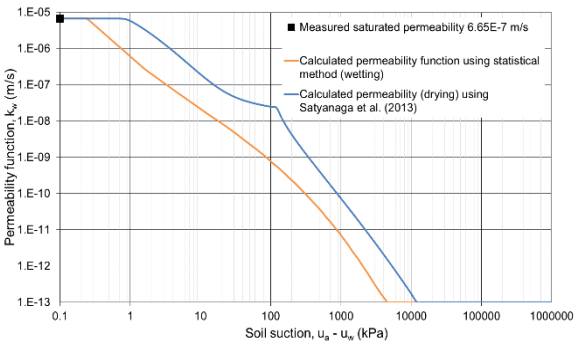

Fig. 14 Permeability curves for drying and wetting SK

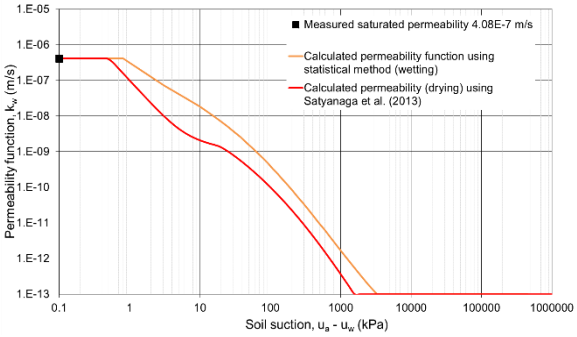

Fig. 15 Permeability curves for drying and wetting SKM

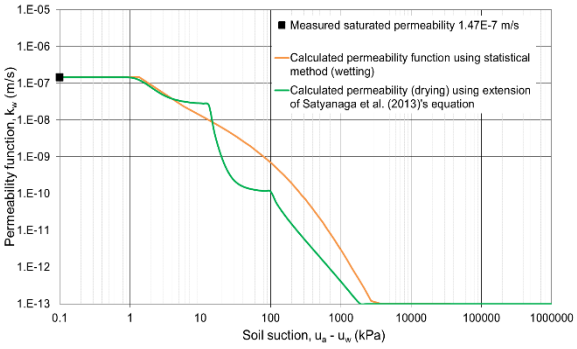

Fig. 16 Permeability curves for drying and wetting SKAC

Observing Figs 13, 14, and 15, the permeability

functions of SK and SKM have two sub-curves, while SKAC has three sub-curves, as SK and SKM exhibit bimodal drying SWCC, while SKAC exhibits trimodal drying SWCC. For the wetting cycle, the permeability functions of all three specimens (SK, SKM, and SKAC) show a single curve due to the unimodal wetting SWCC. The coefficient of permeability begins to decrease at matric suction close to the AEV of the respective soil specimens, which indicates the start of desaturation of the soil specimens. This is because air begins to penetrate the pores of the soil specimen and displaces water. As the volume of water in the voids decreases, it would be harder for water to flow through, resulting in a decrease in permeability. Initially, the coefficient of permeability of SKAC decreases gently (starting from 0.8 kPa) and is higher than that of SKM between matric suctions of 1 and 13 kPa. Subsequently, the coefficient of permeability of SKAC decreases rapidly beyond 13 kPa.

5. CONCLUSIONS

Analyses were performed in this study on the laboratory data for SWCC of three samples: SK, SKM, and SKAC. The following conclusions could be drawn:

1. Dual porosity soils exhibited bimodal SWCCs for the drying curves and unimodal SWCCs for the wetting curves (SK and SKM)
2. The addition of activated carbon powder on sand-kaolin mixture (SKAC) could result in a drying SWCC with trimodal characteristics and a unimodal SWCC for the wetting curve.
3. The bimodal and trimodal SWCC characteristics can be modelled successfully using Satyanaga's (2013) equation.
4. When compared to SKM and SKAC, SK showed the highest permeability function across the whole suction range due to a lower percentage of fines.

Although this study shows that the model performed very well for engineered soil, the application for natural soil should be further explored. For example, the effects of initial moisture content and heterogeneity of the soil on pore size distribution, and also the presence of a contaminant could be investigated more rigorously. There is also a need for further field validation, especially on the hysteretic of the SWCC curve due to wetting and drying conditions.

6. ACKNOWLEDGMENTS

The study is part of collaborative research between Universitas Bina Darma and Universitas Hasanuddin, Indonesia, and Nazarbayev University, Kazakhstan.

7. REFERENCES

[1] Zhai, Q., Rahardjo, H., & Satyanaga, A., Uncertainty in the Estimation of Hysteresis of Soil–Water Characteristic Curve. Environmental Geotechnics Vol. 6, no. 4, 2017, pp.204-213.

[2] Psarropoulos, P.N., Makrakis, N., & Tsompanakis, Y. Climate Change Impact on the Stability of Soil Slopes from a Hydrological and Geotechnical Perspective. GeoHazards Vol. 5, 2024, pp. 1190-1206. https://doi.org/10.3390/geohazards5040056.

[3] Ip, S. C., H. Rahardjo, & A. Satyanaga. Three-Dimensional Slope Stability Analysis Incorporating Unsaturated Soil Properties in Singapore. Georisk: Assessment and Management of Risk for Engineered Systems and Geohazards Vol. 15, no. 2, 2021, pp. 98-112. https://doi.org/10.1080/17499518.2020.1737880

[4] Rahardjo, H., Kim, Y. & Satyanaga, A. Role of unsaturated soil mechanics in geotechnical engineering. International Journal of Geo-Engineering, Vol. 10, No. 8. 2021, pp. 1-23. https://doi.org/10.1186/s40703-019-0104-8

[5] Zhai, Q., Rahardjo, H., Satyanaga, A., & Dai, G., Estimation of Unsaturated Shear Strength from Soil–Water Characteristic Curve, Acta Geotechnica Vol. 15, 2020, pp.3371-3381.

[6] Zhai, Q., Rahardjo, H., Satyanaga, A. Dai, G. & Zhao, XL. The role of pore-size distribution function on the estimation of engineering properties of unsaturated soil. Proc. 7th AP-UNSAT2019. Japanese Geotechnical Society Special Publication Vol. 7, Issue 2. 2019, pp. 382-389 https://doi.org/10.3208/jgssp.v07.061

[7] Satyanaga, A. & Rahardjo, H. Unsaturated shear strength of soil with bimodal soil-water characteristic curve. Géotechnique, Vol. 69, no. 9, 2019, pp. 828-832. https://doi.org/10.1680/jgeot.17.P.108.

[8] Satyanaga, A., Moon, S.-W., Kim, J.R., Stability Analyses of Dual Porosity Soil Slope, Geomechanics and Engineering Vol. 28, no. 1, 2022, pp. 77-87. https://doi.org/10.12989/gae.2021.28.1.077

[9] Fredlund, D.G., and Xing, A., Equations for the Soil-Water Characteristic Curve, Canadian Geotechnical Journal Vol. 31, no. 4, 1994, pp. 521-532.

[10] Satyanaga, A., Rahardjo, H., Leong, E. C., & Wang, J. Y. Water characteristic curve of soil with bimodal grain-size distribution. Computers and Geotechnics, 48, 2013. pp, 51-61. https://doi.org/10.1016/j.compgeo.2012.09.008.

[11] Satyanaga, A., Rahardjo, H., Zhai, Q., Estimation of unimodal water characteristic curve for gap-graded soil, Soils and Foundations, Vol. 57, Issue 5, 2017, pp.789-801. https://doi.org/10.1016/j.sandf.2017.08.009

[12] Li, C., Chen, Y., Xiang, K., Dai, G., Gong, W., Yang, S., Satyanaga, A., Chua, Y.S., Gao, P. & Zhai, Q. (2024) Estimation of the wetting induced settlement of loess soils from the wetting soil-water characteristic curve. Scientific Reports. 14, 31533. https://doi.org/10.1038/s41598-024-83258-x

[13] Hu, D., Kato, S., Kim, B.S., Evaluation of Infinite Slope Stability with Various Soils under Wet-Dry Cycle, International Journal of GEOMATE, Vol. 26, Issue 115, 2024, pp. 89-99. https://geomatejournal.com/geomate/article/view/4501

[14] Bello N, Satyanaga A, Gofar N, & Kim J. Estimation of bimodal soil-water characteristics curve under wetting process. PLoS One Vol. 20, No. 6: e0325646. https://doi.org/10.1371/journal.pone.0325646

[15] Zhai, Q., Ye, W., Rahardjo, H., Satyanaga, A., Dai, G., & Zhao, X. Theoretical Method for the Estimation of Vapor Conductivity for Unsaturated Soil. Engineering Geology 295. 2021: 106447. https://doi.org/10.1016/j.enggeo.2021.106447

[16] Ishii, K., Liu, W., Satoshi Shigemura, and Shoji, K., Relationship between Liquefaction Strength of Sand with Fine Fraction and Various Void Ratios, GEOMATE Journal, Vol. 22 No. 91, 2022, pp. 1–7. https://geomatejournal.com/geomate/article/view/1719

[17] Lee, J.-S., Guimares, M., and Santamarina, J. C., Micaceous Sands: Microscale Mechanisms and Macroscale Response, Journal of Geotechnical and Geoenvironmental Engineering Vol. 133, no. 9, 2007, pp. 1136-1143. DOI: 10.1061/(ASCE)1090-0241(2007)133:9(1136)

[18] Priono; Rahardjo, H., Leong, E.C., and Chatterjea, K., Effects of Mica Content on Hydraulic Anisotropy of Unsaturated Soil, Landslides and Engineered Slopes. Experience, Theory and Practice, 2016, pp. 1675-1683.

[19] Oginni, O. J., Characteristics of Activated Carbons Produced from Herbaceous Biomass Feedstock, Graduate Theses, Dissertations, and Problem Reports. West Virginia University, 2018.

[20] Liu, Z., Dugan, B., Masiello, C. A., and Gonnermann, H. M., Biochar particle Size, Shape, and Porosity Act Together to Influence Soil Water Properties, Plos One, Vol. 12, no. 6, 2017: e0179079.

[21] Brennan, J. K., Thomson, K. T., and Gubbins, K. E., Adsorption of Water in Activated Carbons: Effects of Pore Blocking and Connectivity. Langmuir Vol. 18, no. 14, 2002, pp. 5438-5447.

[22] H. Dong, A. K. Leung, J. Liu, R. Chen, and W. Lui, Microstructural investigation of the unsaturated hydraulic properties of hydrochar-amended soils. Acta Geotechnica, Vol. 19, no. 2, 2024. pp. 833–853, doi: 10.1007/s11440-024-02254-7

[23] Taghizadeh-Toosi, A., Hansen, E.M., Olesen, J.E., Baral, K.L. & Petersen, S.O. (2022). Interactive effects of straw management, tillage, and a cover crop on nitrous oxide emissions and nitrate leaching from a sandy loam soil. Science of The Total Environment. Vol. 828, 2022, 154316, https://doi.org/10.1016/j.scitotenv.2022.154316.

[24] Wei, B., Peng, Y., Lin, L., Zhang, D., Ma, L., Jiang, L., Li, Y., He, T., & Wang, Z. (2023). Drivers of biochar-mediated improvement of soil water retention capacity based on soil texture: A meta-analysis, Geoderma, Vol. 437, 2023, 116591, https://doi.org/10.1016/j.geoderma.2023.116591

[25] Zhai, Q., Ye, W. Rahardjo, H., Satyanaga, A. Dai, G., and Zhao. X., Theoretical Method for the Estimation of Vapor Conductivity for Unsaturated Soil. Engineering Geology 295, 2021, pp. 106447.